Deformation and damage evolution of a full-scale adhesive joint between a steel bracket and a sandwich panel for naval application

Jaiswal, Pankaj R; Kumar, R Iyer; Saeedifar, M; Saleh, MN; Luyckx, Geert; Waele, W De

DOI
10.1177/0954406220947122

Publication date
2020

Document Version
Final published version

Published in
Proceedings of the Institution of Mechanical Engineers, Part C: Journal of Mechanical Engineering Science

Citation (APA)
Jaiswal, P. R., Kumar, R. I., Saeedifar, M., Saleh, MN., Luyckx, G., & Waele, W. D. (2020). Deformation and damage evolution of a full-scale adhesive joint between a steel bracket and a sandwich panel for naval application. *Proceedings of the Institution of Mechanical Engineers, Part C: Journal of Mechanical Engineering Science*, *235*(3), 571-584. https://doi.org/10.1177/0954406220947122

Original Article

Institution of MECHANICAL ENGINEERS
Journal of MECHANICAL ENGINEERING SCIENCE

Proc IMechE Part C:
J Mechanical Engineering Science
0(0) 1–14

DOI: 10.1177/0954406220947122
journals.sagepub.com/home/pic
SAGE

Deformation and damage evolution of a full-scale adhesive joint between a steel bracket and a sandwich panel for naval application

Pankaj R Jaiswal[1], R Iyer Kumar[1], M Saeedifar[2], MN Saleh[2], Geert Luyckx[3] and W De Waele[1]

Abstract

The increasing interest for the application of adhesive joints in naval superstructures motivates researchers to gain an in-depth understanding of the mechanical behaviour and failure mechanisms of these joints. This work reports on an experimental study of the deformation behaviour and damage evolution of a full-scale multi-material joint using different instrumentation techniques. Adhesively bonded joints of steel to sandwich panel components have been subjected to quasi-static tensile tests during which the global deformation of the joint and local strain distributions were monitored using digital image correlation (DIC). During one particular tensile test, fibre optic Bragg sensors (FBG) were also applied to the specimen's surface at different locations in order to quantify the evolution of local strains. Additionally, acoustic emission (AE) sensors were installed in order to monitor damage initiation and evolution with increasing levels of imposed deformation. This test showcased adhesive failure at the interface of the steel adherend and the adhesive, while cohesive failure was observed within the adhesive and skin failure at the interface between adhesive and the composite skin of the sandwich panel. The post-mortem observed failures modes were compared to the acoustic events that originated during the test due to damage initiation and propagation within the joint. The evolution of the different sensor signals, i.e. the damage expressed as cumulative AE energy and local strains measured with Bragg sensors and DIC, are mutually compared and acceptable correlation is found.

Keywords

Adhesive, joints, multi-material, acoustic emission, failure mode, damage characterisation, digital image correlation, fibre optic Bragg sensors

Date received: 20 April 2020; accepted: 10 July 2020

Introduction

Adhesively bonded joints are suggested for light-weight structures used in the automotive and aero-nautical sector where traditional fasteners are discouraged as a consequence of the necessity to join new and dissimilar materials.[1] In recent years, the use of metal-to-composite adhesive joints has expanded in maritime industries as well. As the application of adhesive joints possesses many desirable mechanical properties such as high strength to weight ratio,[2] good fatigue resistance properties,[3] high toughness and low-stress concentration[4] etcetera, they received significant attention of shipbuilding industries in the last few decades.[5] However, the integrity and damage mechanisms of adhesive joints are significant issues in naval industries,[4] and depend on specific parameters like service conditions, production of joint,[6,7] thickness of adherend and adhesive[8,9] and environmental conditions.[2] Numerous scientific studies have been conducted with focus on the durability of adhesive joints in the presence of water, salinity, temperature, fire and ultraviolet radiation[10] and their damage

[1]Soete Laboratory, Department of Electromechanical Systems and Metal Engineering (EMSME), Ghent University, Ghent, Belgium
[2]Structural Integrity & Composites Group, Faculty of Aerospace Engineering, Delft University of Technology, Delft, The Netherlands
[3]Com&Sens, Gent, Belgium

Corresponding author:
Pankaj R Jaiswal, Ghent University Faculty of Engineering and Architecture, Technologiepark-Zwijnaarde, 46 Flex Office 2, Gent 9000, Belgium.
Email: pankaj.jaiswal@ugent.be

mechanisms.[2,11–13] The results demonstrate that the most severe damage occurs at the adhesive/adherend interface.[14] Different environmental exposure can cause a change in the failure mode of the joint. In order to understand the complete behaviour and failure mode of multi-material adhesive joints, one can implement non-destructive testing (NDT) techniques for in-situ evaluation of the damage.

Digital image correlation (DIC) is an advanced non-contact optical technique to measure the evolution of deformation at the surface of components. Kumar et al.[15] successfully applied the technique to analyse the evolution of peel and shear strain in single lap adhesive joints of carbon fibre reinforced plastic (CFRP) coupons and the evolution of zero volume disbonds in single lap adhesive joints (SLJ) of glass fibre reinforced composite (GFRP) coupons subjected to tensile load.[16] In both cases, bonding was performed using a structural epoxy Araldite AV138. Crammond et al.[17] implemented DIC to analyse local strains in a GFRP double butt strap joint bonded with a structural epoxy paste Araldite 2015, during tensile testing. They demonstrated that localised strain distributions at mesoscopic scale around the discontinuity between the adherends could be effectively evaluated using high magnification levels. Kashfuddoja et al.[18] conducted an assessment of thickness displacement and local strain field in the thin adhesive layer of a single sided patch repaired CFRP panel subjected to tensile load. DIC allowed an accurate characterisation of global and local strain (longitudinal, peel and shear strain) in the thin adhesive layer and monitoring of damage in the patch repaired joints.

In order to gain an in depth understanding of adhesive and adhesive joint behaviour under different loading conditions, several researchers have evaluated strain using optical fibre Bragg (FBG) sensors and correlated the results with DIC measurements. Mulle et al.[19] monitored the surface strain of a glass epoxy sandwich structure subjected to tension by means of FBG sensors attached to the surface with high and low viscosity adhesive. FBG strain results were compared to DIC measurements; the low viscosity adhesive resulted in better strain measurement than the high viscosity adhesive. Dvořák et al.[20] compared FBG, DIC and strain gauges by measuring the strain of a carbon/epoxy composite specimen subjected to a tensile test till failure. The results showed a good agreement for all three strain measurement techniques, with a maximum difference of 4%. Mulle et al.[21] also studied the mechanical behaviour of thick beam type specimens subjected to three point and four point bending tests. Several FBG sensors were embedded at different levels of ply stack while full-field surface strain measurement was carried out using DIC. Longitudinal strain measurement with DIC and FBG over the thickness of the upper part of the specimen showed a perfect agreement between both techniques; in the lower part of the specimen some values differed by less than 10%. Bernasconi et al.[22] studied strain profile measurement and crack propagation in SLJ specimens of CFRP laminates adhesively bonded by structural epoxy Scotch Weld 9323 B/A, subjected to tensile and fatigue loadings. FBG and strain gauges were embedded at the back face of the adherend near the overlap region. The results were compared with finite element simulations and DIC results; a good agreement was found.

In recent years, the acoustic emission (AE) technique has gained popularity for damage characterisation. It is often used for online inspection of damage and the categorisation of damage mechanisms of bonded structures. Acoustic emission is very sensitive to the internally generated stress waves resulting from any change in the joint. This feature has received attention for inspecting the failure mode of steel-to-composite adhesive joint during mechanical tests.[23,24] However, it remains a significant challenge for engineers to recognise and classify the failure modes of adhesive joints with AE. Saleh et al.[23] have studied the failure mode of a double lap adhesive joint using AE, where a steel adherend is bonded to two CFRP traps using both epoxy and MMA based adhesive with an 8 mm thickness. DIC was also used for continuous monitoring of the joint cross-section and for crack detection during the tension test. A good correlation between DIC and AE for damage detection was established. Young et al.[24] proposed the AE method to detect damage for three different types of joints; i.e. a double lap adhesive, a mechanical and a hybrid (adhesive + mechanical) joint. A high-speed camera and AE signal analyser were utilised to observe the damage and it was shown that AE could classify the failure modes of the joints appropriately. Angelopoulos[25] has applied AE for monitoring the damage onset and subsequent evolution of a full-scale steel-to-composite adhesive joint for a naval structure. He studied various approaches for AE signal post-processing and its correlation with the evolution of damage. Manterola et al.[26] proposed AE for detection of mode-I crack growth in double cantilever beam (DCB) specimens bonded with both rigid and flexible adhesive. The nature of cracks could be determined based on the correlation of AE data, numerical models and visual observation. Moreover, Liu et al.[27] monitored mode-I and mode-II progressive failure in double cantilever beam (DCB) and end notch flexure (ENF) type composite adhesive joint specimens using AE. Analysis of failure mechanisms was also done using high-speed camera images and scanning electron microscopy. The authors demonstrated that progressive failure of the joint could be monitored using the AE amplitude spectrum distribution; adhesive failure in mode-I and accumulation of damage at the edge of the joint in mode-II were observed. Xu et al.[28] investigated the fracture mode of a single lap composite adhesive joint using cluster

analysis and combining time and frequency domain analysis to deal with AE activity. Adhesive failure and composite delamination in an SLJ specimen with extreme damage was identified through wavelet analysis. Similarly, Bak et al.[29] have distinguished failure modes for three different types of SLJ specimens; adhesively bonded, riveted and hybrid joints subjected to a quasi-static tension test. It resulted in interlaminar shear failure in the riveted joint, in adhesive failure, shear failure and (light) fibre tear failure for the adhesive joint; and fibre tear failure was observed for the hybrid joint. All dominant failure modes of the three different joints were confirmed through fast Fourier transformation (FFT) of the AE activity.

In order to utilise the full capacity of a multi-material adhesive joint in shipbuilding, it is necessary to gain a deep understanding of the damage mechanisms and strain distribution in the joint. In this paper, the evolution of deformation and damage in an adhesive joint of a steel bracket to a sandwich panel has been monitored using different instrumentation techniques, namely acoustic emission, digital image correlation and fibre optic Bragg sensors. This work is part of the Qualify project of Interreg2Seas Mers Zeeen. The main goal of the project is to provide qualification guidelines for real scale adhesive joints for lightweight and safe maritime transport.[30]

Joint configuration and materials

The production of the full-scale adhesive joint was done in actual shipyard conditions (Damen Schelde Naval Shipbuilding, the Netherlands). For the final manufacturing of the full-scale joint, a sandwich panel was placed inside a steel profile (shipbuilding steel AH36), and the 10 mm gap in between panel and steel flanges was filled with a two-component methyl methacrylate (MMA) adhesive. The gap between the bottom part of the steel and the sandwich panel was filled with foam to avoid damage and crack initiation due to impact loads. The full-scale adhesive joint specimen was produced as a section with a width of 100 mm cut by water jet cutting from a large shipyard hybrid panel. The final appearance of the full-scale adhesive joint and its global dimensions are shown in Figure 1.

The selection of adhesive was based on its favourable mechanical properties like high toughness and flexibility, shock resistance, excellent impact and peel strength, as these are considered dominant characteristics of an adhesive joint used in shipbuilding industries.[31,32] The nominal mechanical properties of steel AH36[33] and adhesive MMA[34] are summarised in Table 1.

Good alignment of the specimen is a dominant factor to avoid geometrical eccentricity while applying the tensile loading. For that purpose, a suitable fixture had to be designed and manufactured. The upper end of the specimen is hold by employing a knuckle pin with a double forked end, while at the other side the specimen flange was extended to obtain a sufficient area for gripping in the hydraulic clamps of the testing machine. The flange was connected to the extended steel part of the fixture by bolting and fillet welding. The detrimental effect of stress concentrations due to welding has been minimised by a shot peening operation. A schematic drawing and photograph of the specimen unit fixture are, shown in Figure 2.

Experimental procedure

Two quasi-static tensile tests have been carried out using a servo-hydraulic testing machine MTS 810 with a 1000 kN load cell capacity. The tests were performed at room temperature and a constant displacement rate of 1 mm/min up till complete rupture. The first test mainly served as a trial test to evaluate the test methodology and robustness of the fixtures.

Table 1. The main mechanical properties of steel and MMA adhesive.

Property	Steel (AH36)	MMA
Tensile strength (MPa)	400–550	12–15
Yield stress (MPa)	350	–
Young's modulus, E (GPa)	200	0.207–0.276
Poisson's ratio	0.26	–
Lap Shear strength [MPa]	–	16–19

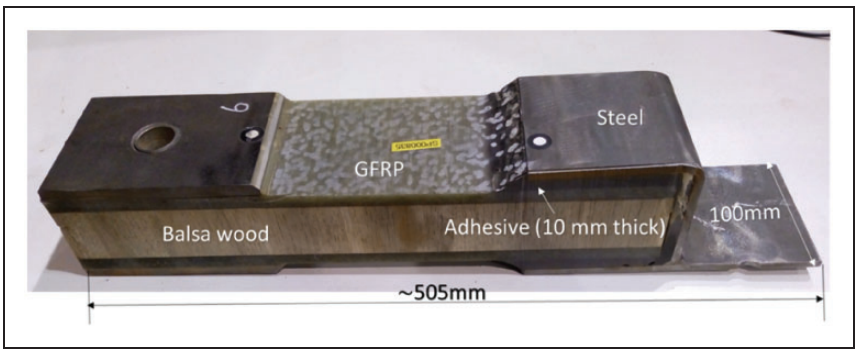

Figure 1. Fabricated full-scale adhesive joint specimen.

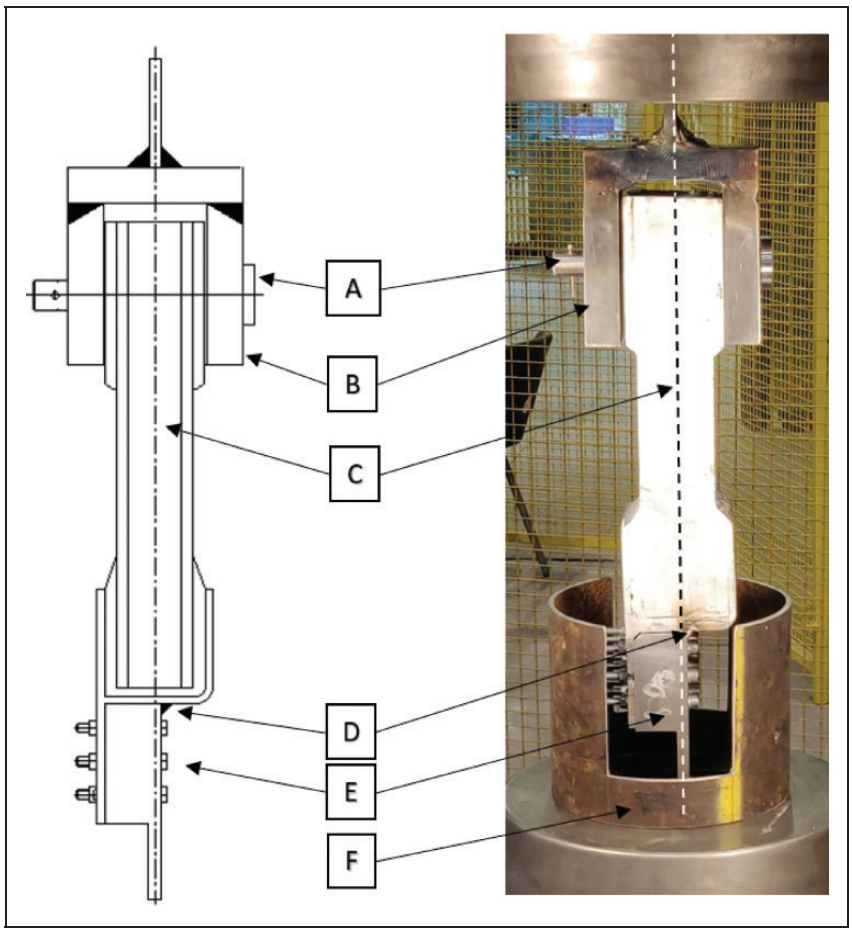

Figure 2. Schematic diagram and photograph of specimen and fixture mounted in the tensile test machine. (a-Knuckle pin, b-Double forked end, c-Alignment (centre) line, d-Fillet weld, e-Single forked end, f-Protective shield.).

The second test will be reported in detail in this paper. As introduced above, three different NDT techniques (i.e. DIC, FBG and AE) for strain and damage measurement have been implemented. The surface strain on the region of interest of the specimen was continuously monitored by DIC. Local values of strain were monitored and recorded by FBGs surface mounted on the composite skin and steel part of the specimen. The acoustic activity of the joint was recorded by placing AE sensors on the GFRP skin and steel part of the joint. A detailed explanation of the applied instrumentation is presented in the following section. Figure 3 provides a view of a mounted test specimen and the position of AE sensors, FBG sensors and DIC speckle pattern on the surface of the specimen. The DAQ system of the MTS testing machine was used to record load and crosshead displacement data during the tests.

Digital image correlation (DIC)

DIC is a contactless optical technique to measure the displacement of a deforming body. In this work, it is used to quantify comprehensive surface deformation of the bulk adhesive layer and steel material. The stereoscopic DIC system consists of two 14 bit high-speed digital cameras (Limess). The resolution of both cameras is 5 MP (2452×2054 pixels), additional lenses were mounted to achieve the best possible resolution. VIC-Snap software is used to acquire synchronized images from both cameras. The speckle size was determined based on the interest area of the specimen; the optimal value is 0.10 mm/speckle. Before the quasi-static tensile test, DIC calibration was performed by obtaining the recommended calibration score (i.e., less than 0.03 error per pixel). In total, hundreds of images were captured at a rate of 1 picture per second during the test. Eventually, the post-processing of images was done by selecting a subset size of 29×29 pixels with a step size (pitch of subset) of 7 pixels in the DIC software VIC-3D software used for post-processing and 3D measurement of displacement and strain.

Fibre optic Bragg sensors (FBG)

FBG technology is not a novelty, and FBG sensors have been used in commercial applications for already more than three decades. FBGs can be applied as optical strain gauges, in surface mounted configuration or even as an embedded sensing

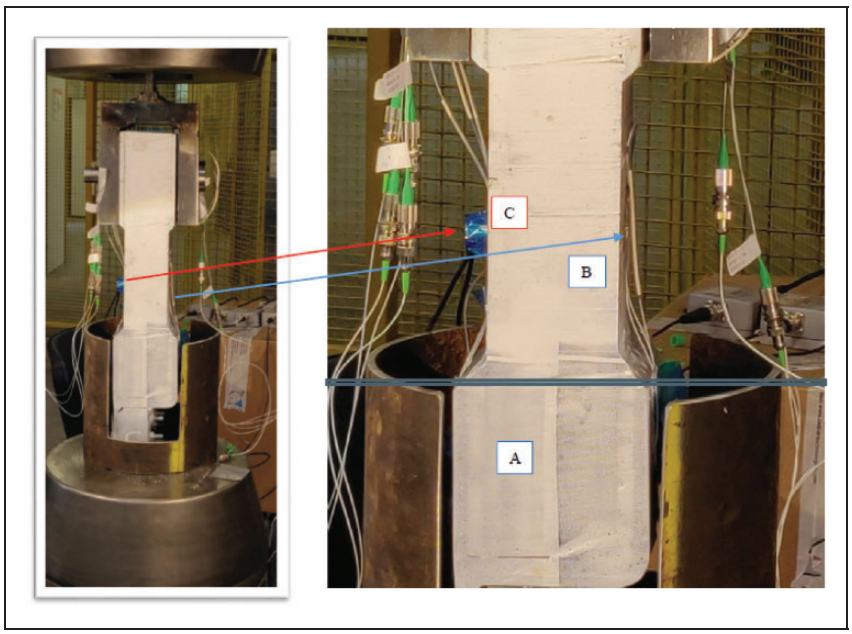

Figure 3. Laboratory setup with mounted full-scale joint and applied instrumentation; DIC speckle pattern across the entire cross section (a) and surface mounted fibre optic Bragg sensors (b) and acoustic emission sensors (c).

element (e.g. in composite materials). The main difference between an electrical strain gauge and an FBG is the fact that the FBG is a passive optical component with absolute sensor properties (i.e. no drift in time). This means that once it is calibrated for a specific temperature region, there is no need to re-calibrate it, which is a major advantage once it is in service.

The technology is based on the Bragg principle, which is explained as follows. When sending broadband light in an optical fibre with Bragg grating, a certain part of the light ('colour') is back reflected. When the fibre is being elongated, the grating period will be strained, and the refractive index of the fibre will change as well. As a consequence, a positive Bragg peak shift is induced ('colour change'). An interesting aspect is the multiplexing ability of FBG sensors. One can put more than 20 FBGs in a series configuration in one optical fibre (or channel), with each sensor having its unique reflected Bragg wavelength (i.e. 'colour'). As such a multichannel optical interrogation system can easily monitor hundreds of FBG sensors in one sensing network using a limited number of optical lines.

In this work, optical fibres with FBG sensors of 8 mm length were installed (by glueing) to measure the strain at various locations on the composite (GFRP) skin of the sandwich panel and the steel surface of the specimen, as shown in Figure 4.

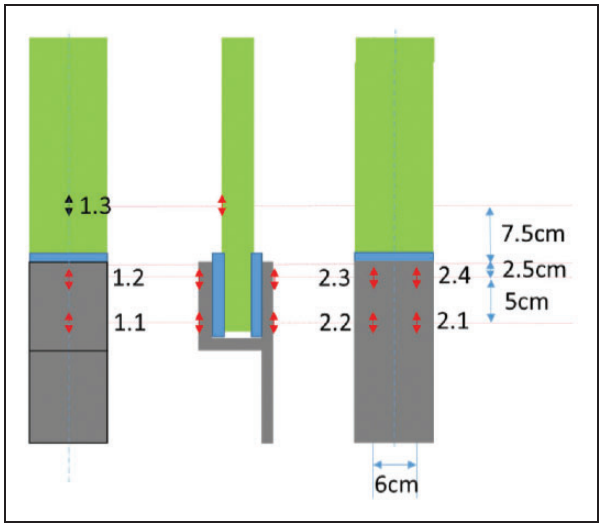

Figure 4. Locations of FBG sensors on composite skin (1.3) and steel flange (front side 1.2 and 1.1) (back side 2.1 to 2.4).

Acoustic emission (AE)

In order to capture the AE signals originated from the joint during the tensile test, five AE sensors were placed on the surface at pre-defined positions. As depicted in Figure 5, three sensors were placed at the lower part of the joint, two on the steel sides (i.e sensors 1 and 3) and one on the foam core (i.e sensor 2). The other two sensors were placed at mid-height of the joint, one on the foam core (i.e sensor 4) and the other on the GFRP skin (i.e sensor 5).

The AE sensor used in this study was VS900-M produced by Vallen Systeme GmbH. The operating frequency range of the sensor was 100–900 kHz. In order to amplify the captured signals, a pre-amplifier with a gain of 34 dB was used. The AE threshold and sampling rate were set to 50 dB and 2 MHz, respectively. A sufficient coupling between the sensor and the surface of the joint was achieved

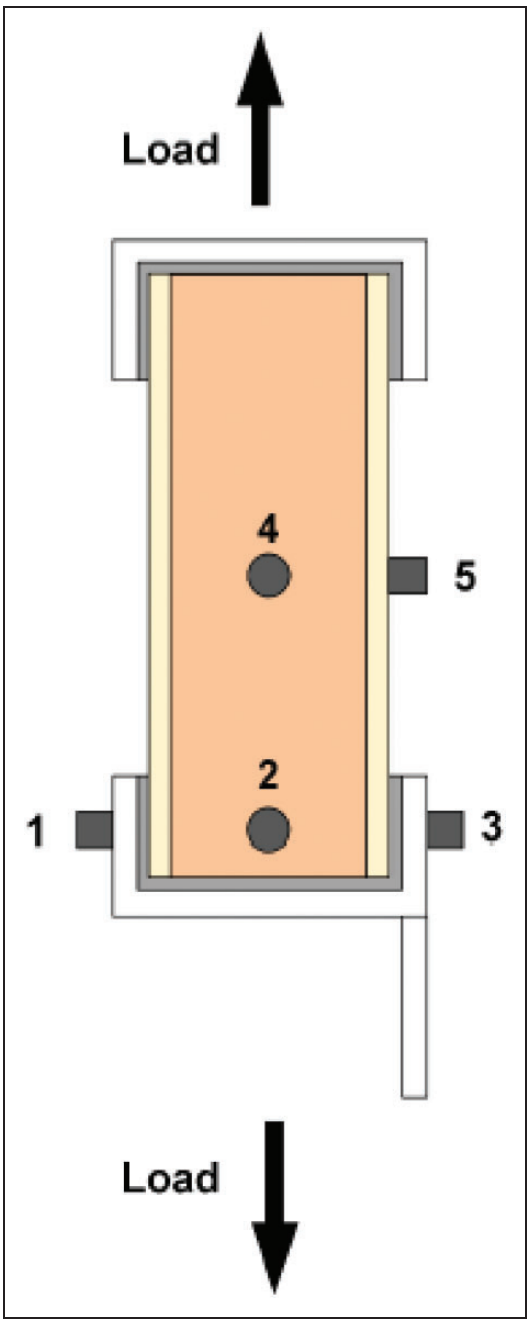

Figure 5. The arrangement of the AE sensors on the joint (Sensors 1 and 3 on steel flange, sensors 2 and 4 on foam core, sensor 5 on GFRP skin).

using ultrasound gel. The performance of the AE system was validated before each test by conducting a standard pencil lead break procedure.[35]

Result and discussion

This section is divided into two subparts. First, the deformation behaviour of the tensile loaded joint is evaluated based on the DIC measurements and the readings from the FBG sensors. Second, the AE signals are discussed and related to observed damage during the tensile test.

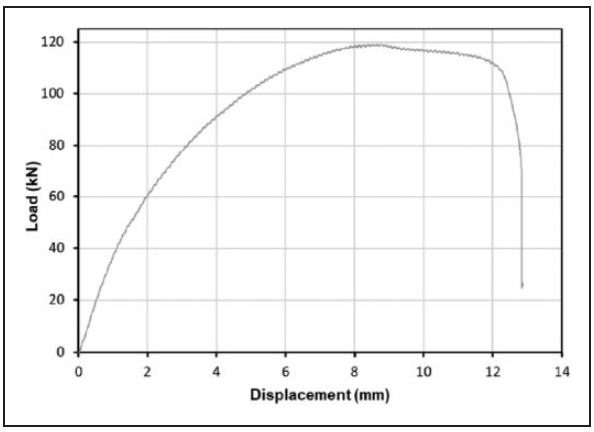

Figure 6. Load-displacement curve of the full-scale adhesive joint specimen.

Characterisation of tensile behaviour

Figure 6 shows the load-displacement curve of the tested joint. The curve displays a linear evolution at the start of the test; around a tensile load of 40 kN the curve noticeably starts to deviate from a linear evolution due to the viscoelastic behaviour of the MMA adhesive. During the further evolution of the test, the nonlinear behaviour becomes more pronounced and displacement significantly increases at a more or less constant load till failure. The ultimate load recorded for this specimen was around 120 kN. The shear strain evolution at the cross-section surface of the specimen was obtained by post-processing DIC images and is illustrated for five different moments during the test, as shown in Figure 7. A general trend of increasing deformation with increasing tensile load can be observed. Image A is the initial image just before the beginning of the test, thus corresponding to zero shear strain. From a crosshead displacement of 2 mm (image B) both bond lines show a significant shear strain development with the maximum values occurring at the centre of the bond lines.

In image C the damage has initiated by tearing and debonding of the adhesive at the interface of steel and adhesive at the top-right side of the sample. Image D corresponds to ultimate load around 120 kN; tearing and debonding of the adhesive at the top of the steel-adhesive interface at both sides of the joint including debonding of adhesive-composite interface at the left top of the joint were observed. Finally in image E, tearing of the adhesive and debonding at the interface of adhesive and composite were observed at both sides of the specimen, as well as debonding at the steel–adhesive interface at the top right side of the specimen. Near the end of the test the shear strain values start to decrease due to unloading of the joint. It can also be observed that the shear strain pattern on image E is less uniform than the patterns observed in images B-D. This is the result of local damage and increased asymmetry in the loading of

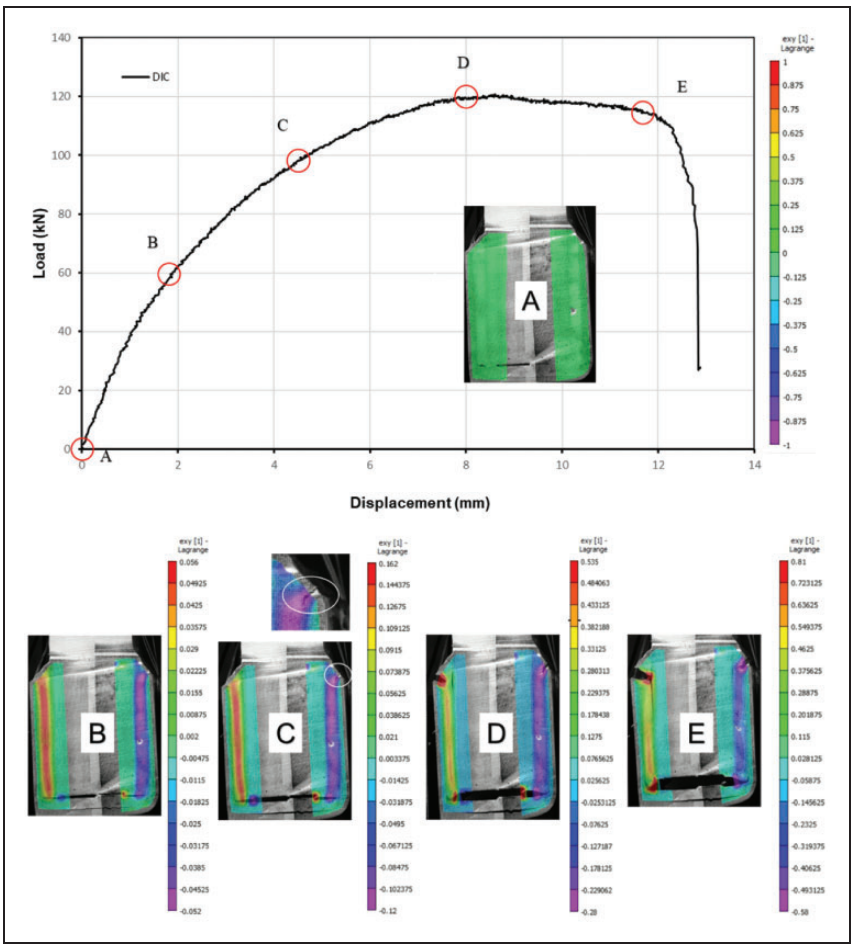

Figure 7. Load-displacement curve and shear strain distribution around the bond line of the specimen at different moments during the test.

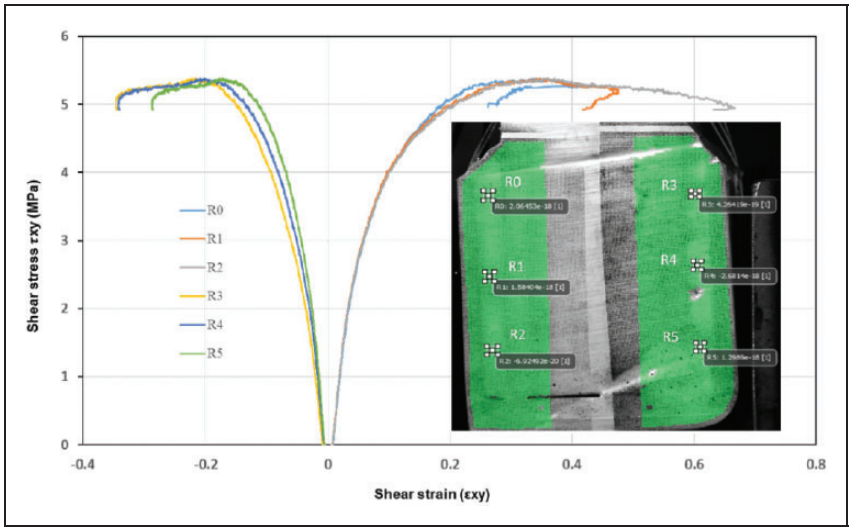

Figure 8. Shear stress-shear strain curves for six different locations in the adhesive of the full-scale joint specimen.

the joint lead. These observations encourage a more detailed strain analysis.

In order to evaluate the local shear strain behaviour within the adhesive, individual plots of shear stress versus shear strain for six different regions (i.e. R0 to R5) at the surface of the adhesive are shown in Figure 8. An inspection block method was used to calculate the local shear strain in the adhesive by means of DIC post-processing. The strain values reported for R0 to R5 are the mean values of the four

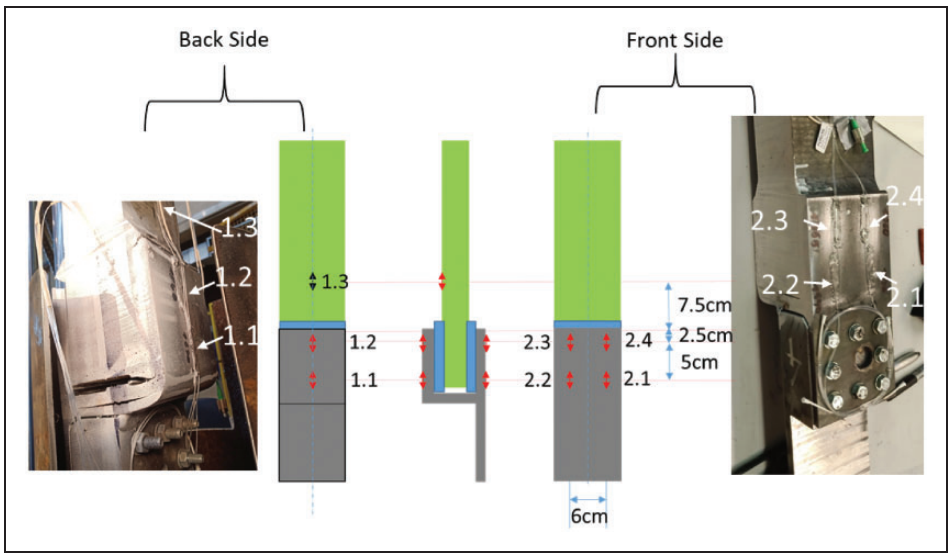

Figure 9. Location of FBGs on the specimen during laboratory test.

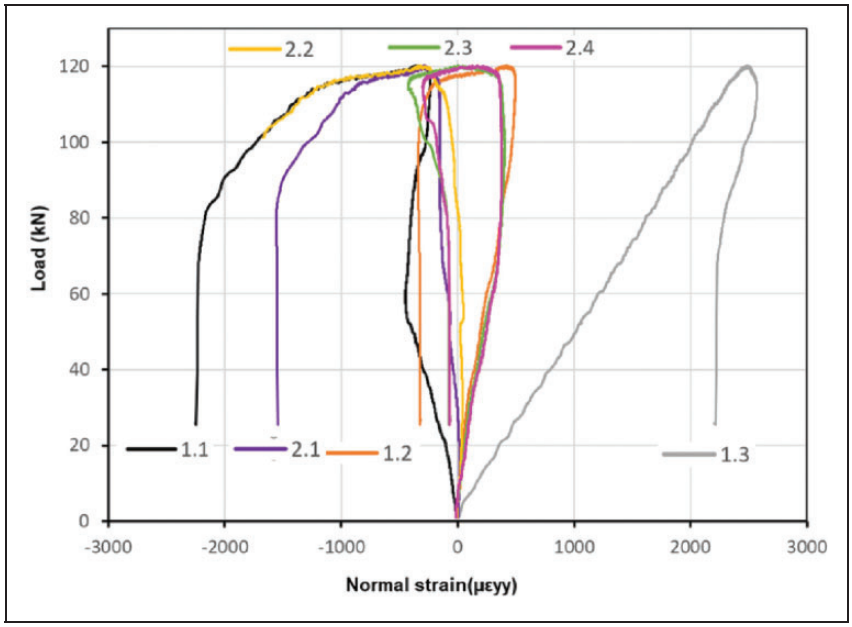

Figure 10. Load versus normal strain profile for each FBG sensor.

corners of each inspection block. The reported shear stress is a global value calculated as the ratio of the applied tensile load to the sheared area of the bond line (i.e. 2 times width multiplied by height). An ultimate shear stress value of 5.4 MPa was calculated.

The shear strain values in the adhesive at the left side of the joint (locations R0, R1, R2) show an identical evolution during most of the test; only close to failure values start to diverge. The failure strains increase from top to bottom of the bond line. This is hypothesized to be due to the closer proximity of R0 to the region of damage and thus partial relaxation of the stresses in the adhesive. The evolution of shear strain values for the regions at the right side of the joint are again similar, although not identical. This is hypothesized to be caused by bending of the right steel flange during the test since it is not directly in line with the load introduction. The failure strains at the right side (R3, R4, R5) are significantly lower than these at the left side (R0, R1, R2).

Also, the normal strain in axial direction has been calculated at the above mentioned regions of interest. The normal strain values are an order of magnitude lower than the shear strain values, demonstrating the predominant shear loading of the adhesive.

In total, seven FBG sensors have been installed at the front and backside of the tested joint. Six sensors were installed on the steel flange (i.e. 1.1, 1.2, 2.1, 2.2, 2.3, 2.4) and one sensor was installed on the

composite skin (i.e. 1.3). The locations of the installed FBG sensors are shown in Figure 9.

The load versus normal strain curves have been plotted for each FBG sensor in Figure 10. The load-strain responses for FBG sensors 2.3 and 2.4 (i.e. sensors mounted at the top of the front face of the specimen) exhibit a functional coherence and both show a linear evolution of strain till 60 kN that subsequently turns into identical non-linear behaviour till failure. Sensor 1.2, which is mounted at the top of the back face, shows an almost identical evolution of strain. These observations are very similar to the load-displacement curve shown in Figure 7 and illustrate the perfect transfer of surface strain to the optical sensors. The load-strain responses for FBG sensors 2.1 and 2.2 (i.e. sensors mounted at the bottom of the front face of the specimen) are similar to each other, but the strains remain very low during the entire loading scheme. They also show an at first sight unexpected evolution towards compressive strains. This is even more pronounced for sensor 1.1 at the back of the specimen. Visual observations of the specimen during tensile loading revealed very severe deformation of the bend region of the steel bracket from the first loading onwards. This is attributed to the low stiffness of the steel plates as compared to the global stiffness of the specimen and due to asymmetric geometry combined with eccentric loading of the joint near the bottom fixture. As a result pronounced out-of-plane bending on top of the axial deformation near the bottom of the joint occurred, which is hypothesized to be the root cause of the load-strain responses observed for sensors 1.1, 2.1 and 2.2. The response obtained from the FBG sensor 1.3 glued to the GFRP plate shows a perfect linear evolution until failure of the specimen. Indeed, during the entire test the very stiff GFRP plate was only elastically deformed; failure of the joint occurred due to plastic deformation of the steel bracket and tearing and debonding of the adhesive.

In order to evaluate the correlation between DIC and FBG, two inspections blocks for DIC post-processing have been defined at the steel surface and close to the locations of FBG sensors 1.2, 2.3 and 2.4.

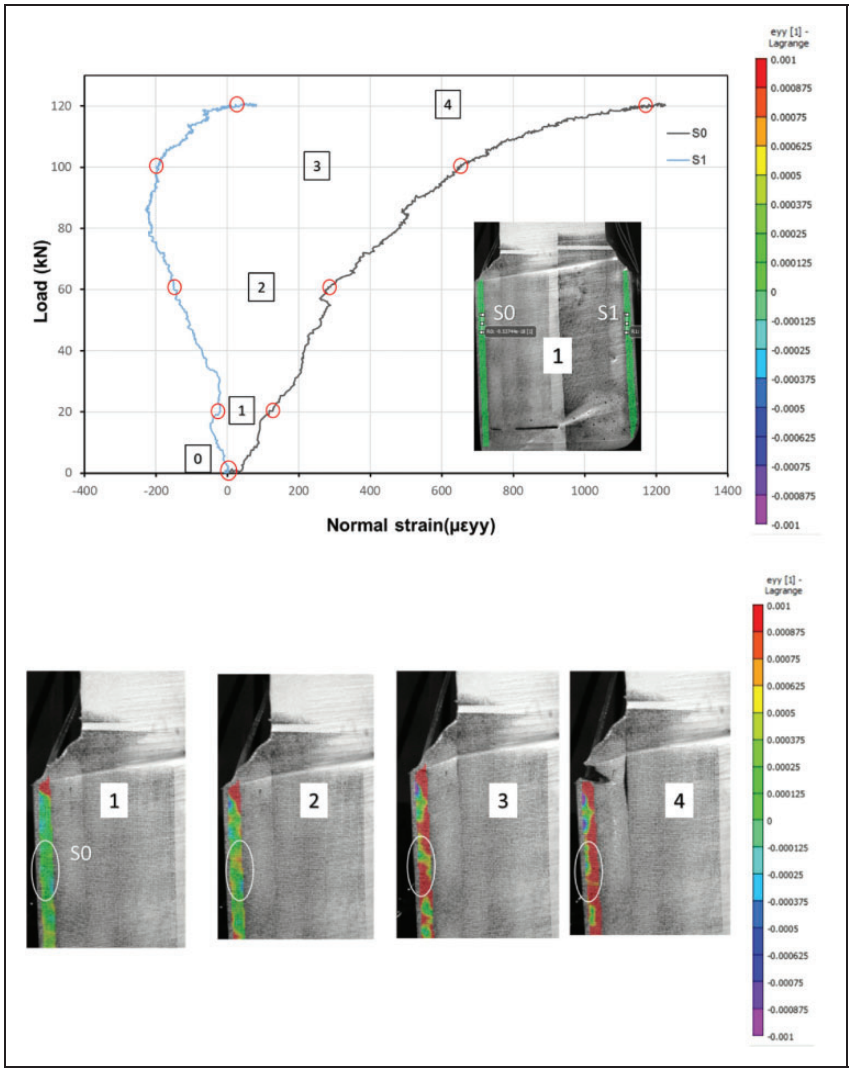

Figure 11. Load versus normal strain curves for DIC inspection blocks (S0 and S1) on the steel surface at the top part of the joint.

The length and pitch of the inspection blocks were approximately the same as the FBG sensors. Since the close proximity and comparable gauge length of DIC and FBG, their responses are expected to show similar (but not identical) trends. It is important to note that the FBGs measure normal strain (in y-direction) and thus also normal DIC strains will be reported. Only the DIC inspection block at the front face (at the same side and height as sensors 2.3 and 2.4) yielded reliable results. The DIC data from the inspection block at the back face showed a lot scatter, most probably because of insufficient quality of the speckle pattern near the edge of the specimen. Load versus normal strain response for the DIC inspection blocks (S0 and S1) and the three FBG sensors mounted at the same height (1.2, 2.3 and 2.4) are shown on Figure 11. Also shown are DIC images of normal strain in the top part of the front steel flange at four different load levels.

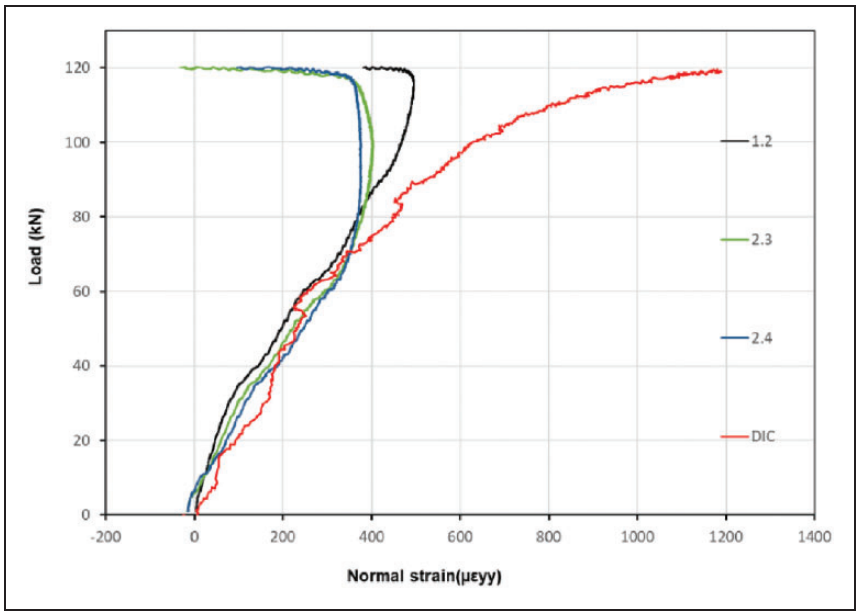

Figure 12. Load versus normal strain curves for DIC inspection block and FBG sensors (2.3, 2.4 and 1.2) on the steel surface at the top part of the joint.

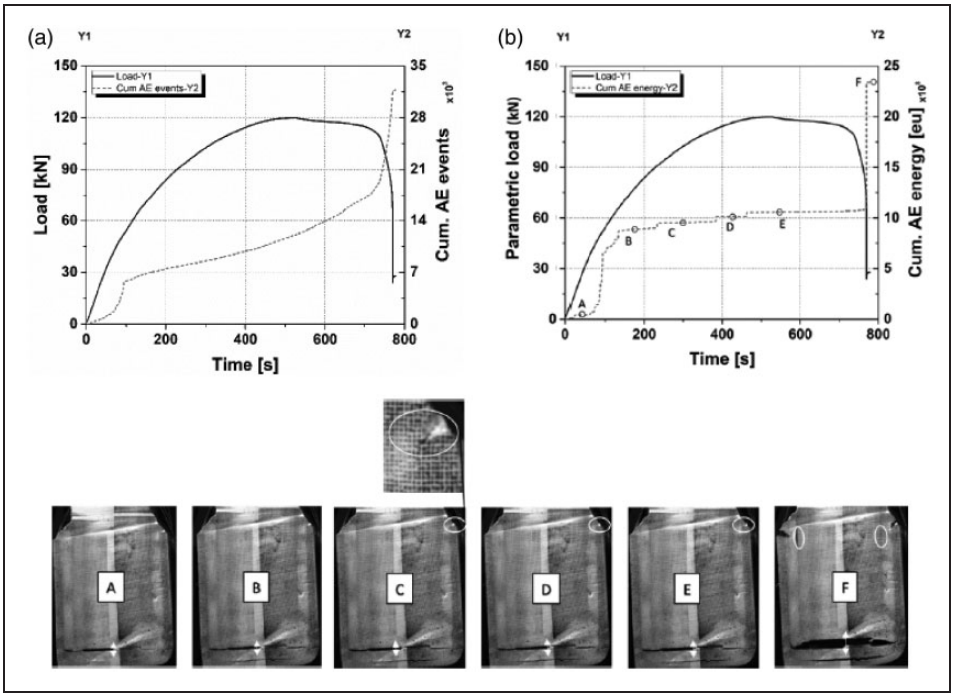

Figure 13. The cumulative AE events (a) and energy curves (b) measured during tensile testing of the full-scale joint.

A very good match between DIC and FBG sensors can be observed for a tensile load up to around 70 kN. Beyond this level, i.e. when the load-displacement curve on Figure 12 becomes highly non-linear, the DIC and FBG data start to deviate significantly. The DIC strains keep on increasing, whilst the FBG strains remain more or less constant.

Analysis of AE signals

The AE signals that originated during the tensile test of the full-scale joint were captured by the 5 AE sensors placed on the surface of the joint as depicted in Figure 5. Investigation of the AE behaviour of the joint can reveal valuable information regarding the damage initiation and its evolution at different levels of the applied load. To this aim, the cumulative number of acoustic events and the cumulative energy released by the AE events are summarized in Figure 13.

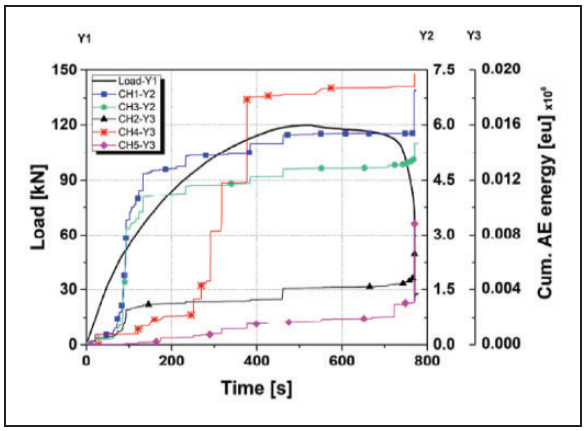

Figure 14. The cumulative AE energy curve for the individual sensors.

As can be seen from the cumulative AE energy, the AE activities started from the beginning of the test and they quickly increased until the load reached approximately 50 kN. Afterwards, the increasing rate of the AE activities considerably decreased till just some moments before the final fracture at which AE activities significantly increased again. The figure also shows several images of the joint at different moments (A-F) during loading. The relation between the evolution in cumulative AE energy and the visual observations of damage will be discussed below.

The cumulative AE energy curves of the individual sensors are detailed in Figure 14. Both sensors 4 and 5 which were far from the damage zone did not show any jump around 50 kN load, while the three sensors placed on the lower part of the joint revealed a significant jump around this load level. This observation could indicate that the damage which occurred at 50 kN load, was mainly concentrated at the lower part of the joint with almost no indication of damage at the middle section of the joint. In addition, as long as the load is less than 50 kN, the energy of the rest of the sensors (1, 2 and 3) increased at the same rate, while the jump in energy captured by the sensors 1 and 3 at this load level is 4 times that of sensor 2. This indicates that, at the load levels less than 50 kN, the damage occurred in the adhesive-rich region at the bottom of the joint (which is equi-distant from the three sensors). When the load reached approximately 50 kN, the damage occurred near the two sides of the joint which were closer to the sensors 1 and 3. This is in agreement with the DIC results depicted in

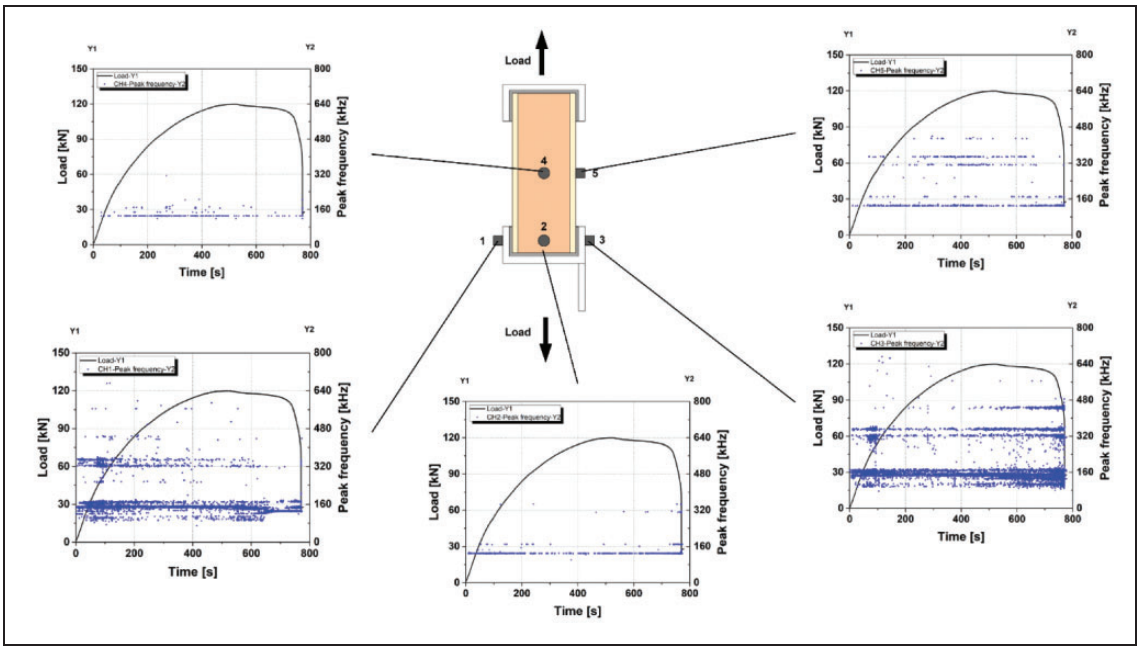

Figure 15. Frequency plots of the signals recorded by the AE sensors.

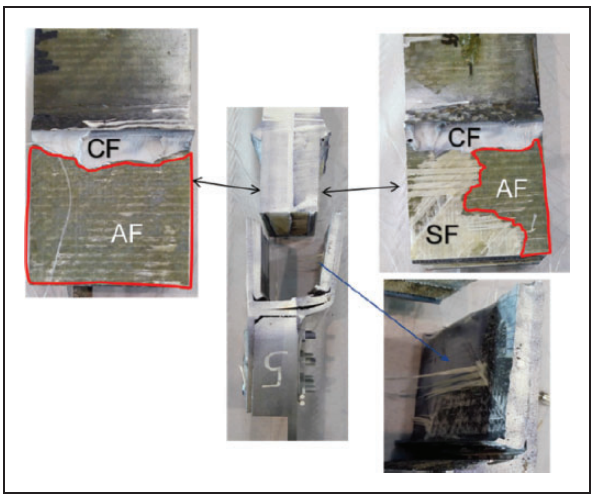

Figure 16. Failure mode of full-scale joint specimen (AF-Adhesive failure, SF-Skin failure and CF-Cohesive failure).

Figure 7. Additionally, six images of the adhesive joint were selected at different loading levels to analyse the change in AE activities presented in Figure 13 (b). As a general trend it was observed that the emission of energy increases with increasing load in terms of a growing gap between the sandwich panel and foam/steel at the bottom of the joint.

Image A is the initial image just at the beginning of the test corresponding to a load of approximately 2 kN. Image B shows the separation of the sandwich panel from the foam and of the foam from the steel at an increased load of 50 kN. Then a minor crack initiated at the interface of steel and adhesive at the right top corner of the joint (see image C), while the gap between steel to foam/sandwich panel further grew slowly as can be seen in images C, D and E. The final jump in the cumulative energy curves of the sensors corresponds to the final fracture of the joint. The tearing of adhesive and debonding at the interface of adhesive-composite at both sides of the specimen can be seen in image F. The frequency distributions of the AE signals recorded by the 5 AE sensors are depicted in Figure 15.

Clearly, the frequency range of the signals recorded by each AE sensor is unique and different from the other ones. This can be attributed to the geometrical position of the sensors and also the constituent material it was placed on. In addition, the different frequency ranges of the AE signals recorded by the sensors may illustrate the occurrence of different damage mechanisms in the joint, as highlighted in Figure 16.

Conclusion

The objective of the presented work was deformation and damage characterization of a full-scale adhesively bonded joint. The specimen consisted of a sandwich core bonded to a steel bracket using an MMA-based adhesive. Three advanced instrumentation techniques were applied, i.e. DIC, FBG sensors and AE sensors. The specimen was subjected to quasi-static tensile loading while DIC and FBG were used to measure the strain at the bond line in a cross-section (DIC) and on outer surfaces of steel and composite (FBG). AE was used for in-situ monitoring of the evolution of damage in the joints. Based on the analysis and comparison of all results, the following conclusions can be drawn.

The local evolution of shear strain in the adhesive bond line was successfully measured using DIC. DIC measurements of shear and normal strain showed that the bond line of the joint was predominantly loaded in a shear mode. The magnitude of shear strain in the adhesive showed an identical pattern and similar evolution for the left and right side bond lines of the tested joint. Due to the asymmetric nature of the failure, the ultimate values of shear strains in the bond line at the right side are significantly lower than these in the bond line at the left side of the joint.

The DIC images also clearly revealed the locations where damage due to tearing of the adhesive or debonding of adhesive and one of the adherends occurred. The load versus normal strain response was successfully recorded at the front and back faces of the specimen by using surface mounted FBG sensors. The strain evolution measured by the sensors mounted at the top of these steel surfaces was in very good accordance with the load-displacement curve measured during the test. Additionally, a good agreement was observed with DIC strain measurement at a similar height on the side surface of the front steel plate.

The evolution of the cumulative energy measured with the AE sensors shows clear indications of damage occurrences that can be linked to visual observations of different types of damage. The sensor location has a clear impact on its sensitivity to damage. It is hypothesized that the frequency content of the AE signal can be linked to the type of damage observed post-mortem (cohesive, adhesive and skin failure were observed at the interface of steel and composite).

Declaration of Conflicting Interests

The author(s) declared no potential conflicts of interest with respect to the research, authorship, and/or publication of this article.

Funding

The author(s) disclosed receipt of the following financial support for the research, authorship, and/or publication of this article: This research was carried out within the project "QUALIFY–Enabling Qualification of Hybrid Joints for Lightweight and Safe Maritime Transport". This project has received funding from the Interreg 2 Seas programme 2014-2020 co-funded by the European Regional

Development Fund under subsidy contract No 03-051and the province of East-Flanders.

ORCID iDs

Pankaj R Jaiswal https://orcid.org/0000-0002-9373-4489
R Iyer Kumar https://orcid.org/0000-0003-1241-2697
M Saeedifar https://orcid.org/0000-0003-4950-3007

References

1. Créac'hcadec R, Jamin G, Cognard JY, et al. Experimental analysis of the mechanical behaviour of a thick flexible adhesive under tensile/compression-shear loads. *Int J Adhes Adhes* 2014; 48: 258–267.
2. Hirulkar NS, Jaiswal PR, Reis PNB, et al. Bending strength of single-lap adhesive joints under hygrothermal aging combined with cyclic thermal shocks. *J Adhes* 2019; 1–5823.
3. Sugiman S and Crocombe AD. The static and fatigue responses of aged metal laminate doublers joints under tension loading. *J Adhes Sci Technol* 2016; 30: 313–327.
4. Zhou W, Liu R, Lv ZH, et al. Acoustic emission behaviors and damage mechanisms of adhesively bonded single-lap composite joints with adhesive defects. *J Reinf Plast Compos* 2015; 34: 84–92.
5. Li X, Li P, Lin Z, et al. Mechanical behavior of a glass-fiber reinforced composite to steel joint for ships. *J Marine Sci Appl* 2015; 14: 39–45.
6. Song MG, Kweon JH, Choi JH, et al. Effect of manufacturing methods on the shear strength of composite single-lap bonded joints. *Compos Struct* 2010; 92: 2194–2202.
7. Markatos DN, Tserpes KI, Rau E, et al. The effects of manufacturing-induced and in-service related bonding quality reduction on the mode-I fracture toughness of composite bonded joints for aeronautical use. *Compos Part B Eng* 2013; 45: 556–564.
8. Taib AA, Boukhili R, Achiou S, et al. Bonded joints with composite adherends. Part I. Effect of specimen configuration, adhesive thickness, spew fillet and adherend stiffness on fracture. *Int J Adhes Adhes* 2006; 26: 226–236.
9. Sugiman S, Salman S, Setyawan PD, et al. Effect of adhesive thickness on the strength of steel-composite joints aged in wet environment. *IOP Conf Ser Mater Sci Eng* 2019; 532: 12007.
10. Jaiswal PR, Hirulkar NS, Reis PNB, et al. Effect of cyclic solar (UV) radiation and temperature on mechanical performance of single lap adhesive joint. In: *2017 international conference on intelligent computing, instrumentation and control technologies (ICICICT 2017)*, Kerala, India, January 2018, pp.182–189. IEEE Xplore.
11. Galvez P, Abenojar J and Martinez MA. Effect of moisture and temperature on the thermal and mechanical properties of a ductile epoxy adhesive for use in steel structures reinforced with CFRP. *Compos Part B Eng* 2019; 176: 107194.
12. Heshmati M, Haghani R and Al-Emrani M. Environmental durability of adhesively bonded FRP/steel joints in civil engineering applications: state of the art. *Compos Part B Eng* 2015; 81: 259–275.
13. Zhang J, Cheng X, Guo X, et al. Effect of environment conditions on adhesive properties and material selection in composite bonded joints. *Int J Adhes Adhes* 2018; 96: 1–7.
14. Goglio L, Rezaei M and Rossetto M. Moisture degradation of open-faced single lap joints. *J Adhes Sci Technol* 2014; 28: 1382–1393.
15. Kumar RLV, Bhat MR and Murthy C. Experimental analysis of composite single-lap joints using digital image correlation and comparison with theoretical models. *J Reinf Plast Compos* 2013; 32: 1858–1876.
16. Vijaya Kumar RL, Bhat MR and Murthy C. Evaluation of kissing bond in composite adhesive lap joints using digital image correlation: Preliminary studies. *Int J Adhes Adhes* 2013; 42: 60–68.
17. Crammond G, Boyd SW and Dulieu-Barton JM. Evaluating the localised through-thickness load transfer and damage initiation in a composite joint using digital image correlation. *Compos Part A Appl Sci Manuf* 2014; 61: 224–234.
18. Kashfuddoja M and Ramji M. Assessment of local strain field in adhesive layer of an unsymmetrically repaired CFRP panel using digital image correlation. *Int J Adhes Adhes* 2015; 57: 57–69.
19. Mulle M, Moussawi A, Lubineau G, et al. Response of fiber Bragg gratings bonded on a glass/epoxy laminate subjected to static loadings. *Compos Struct* 2015; 130: 75–84.
20. Dvořák M, Chlup H, Horný L, et al. Comparison of strain measurement methods: optical FBG sensors, strain gages & digital image correlation. In: *EAN 2012 Proceedings of the 50th annual conference on experimental stress analsis 2012*, Tabor, Czech Republic, October 2014.
21. Mulle M, Zitoune R, Collombet F, et al. Embedded FBGs and 3-D DIC for the stress analysis of a structural specimen subjected to bending. *Compos Struct* 2009; 91: 48–55.
22. Bernasconi A, Kharshiduzzaman M and Comolli L. Strain profile measurement for structural health monitoring of woven carbon-fiber reinforced polymer composite bonded joints by fiber optic sensing using an optical backscatter reflectometer. *J Adhes* 2016; 92: 440–458.
23. Saleh MN, Saeedifar M, Zarouchas D, et al. Stress analysis of double-lap bi-material joints bonded with thick adhesive. *Int J Adhes Adhes. 2019* 2020; 97: 102480.
24. Lee YH, Lim DW, Choi JH, et al. Failure load evaluation and prediction of hybrid composite double lap joints. *Compos Struct* 2010; 92: 2916–2926.
25. Angelopoulos N. *Damage detection and damage evolution monitoring of composite materials for naval applications using acoustic emission testing*. Birmingham: The University of Birmingham, 2017.
26. Manterola J, Aguirre M, Zurbitu J, et al. *Using acoustic emissions (AE) to monitor mode I crack growth in bonded joints. Engineering Fracture Mechanics* 2020; 224: 106778.
27. Liu R, Shen G and Zhang P. Acoustic emission response and progressive failure behaviors of composite adhesively bonded joints loaded by Mode I and II Acoustic emission response and progressive failure behaviors of composite adhesively bonded joints loaded by Mode I and II. *Materials Research Express* 2020; 7: 015307.

28. Xu D, Liu PF, Li JG, et al. Damage mode identification of adhesive composite joints under hygrothermal environment using acoustic emission and machine learning. *Compos Struct* 2019; 211: 351–363.
29. Bak KM, Kalaichelvan K and Jothilingam A. Acoustic emission characterization of failure modes of single-lap joints in glass/epoxy specimens. *Journal of Composite Materials* 2015; 50: 3–23.
30. European Regional Development Fund. Enabling qualification of hybrid structures for lightweight and safe maritime transport, www.interreg2seas.eu/en/qualify (accessed 21 July 2020).
31. Gluegun. Kozłowski M, Bula A and Hulimka J. Determination of mechanical properties of methyl methacrylate adhesive (MMA). *Archit Civ Eng Environ* 2018; 11: 87–96.
32. An introduction to methyl methacrylate adhesives (MMAs), www.gluegun.com/blogs/adhesive-reviews/an-introduction-to-methyl-methacrylate-adhesives-mmas (accessed 21 July 2020).
33. Okawa T, Shimanuki H, Funatsu Y, et al. Effect of preload and stress ratio on fatigue strength of welded joints improved by ultrasonic impact treatment. *Weld World* 2013; 57: 235–241.
34. Saeedifar M, Saleh MN, De Freitas ST, et al. Damage characterization of adhesively-bonded Bi-material joints using acoustic emission. *Compos Part B Eng* 2019; 176: 107356.
35. Boczar T and Lorenc M. Standard guide for determining the reproducibility of acoustic emission sensor response. *Phys Chem Solid State* 2006; 7: 585–588.